



Effects of unbalance orientation on the dynamic characteristics of a double overhung rotor system for high-speed turbochargers

Longkai Wang · Ailun Wang · Yijun Yin · Xing Heng · Miao Jin

Received: 16 May 2021 / Accepted: 14 November 2021 / Published online: 29 November 2021
© The Author(s), under exclusive licence to Springer Nature B.V. 2021

Abstract Part of the same type turbochargers installed on the automobile engines often exhibits considerable sub-synchronous vibration and uncomfortable noise, since the unbalance orientation between the turbine and the compressor impeller may be different. Aiming at this problem in engineering, this paper systematically studies the effect of unbalance orientation of an actual turbocharger rotor-floating ring bearing system. The continuous rotor is discretized by using the FE method combined Guyan DOF reduction. The effectiveness of the TC model is verified by the resonance peak comparisons between the simulation and the test data. On this basis, the unbalance orientation, magnitude and the rotational speed are taken as variables in the simulation performed. The results show that the unbalance orientation is a critical parameter that affects the vibration characteristics. Some certain unbalance orientation is easy to induce the energy transfer between the shaft and the bearings, which is highly related to the first two critical modes. The instability of outer oil-films is responsible to the severe vibration of

turbocharger. A suitable range of unbalance orientation can significantly increase the onset speed of instability and reduce the total vibration level. With the design goal of a high-efficiency turbocharger with low vibration and noise, and minimizing dynamics difference between turbochargers of the same type, it is recommended to keep the unbalance orientation in the range of 0° to 60° .

Keywords Turbocharger · Floating ring bearing · Sub-synchronous Vibration · Unbalance orientation · Vibration difference · Stability

1 Introduction

Exhaust gas turbocharging technology has become an effective measure to improve engine's power performance and reduce energy consumption. In the face of new challenges in energy supply–demand and new trends in international energy development, turbocharging technology will be more widely developed and applied in automobiles, but its smooth and efficient operation must be ensured.

Light-weight turbochargers (TCs) are characterized by high-speed, high-flexibility, high-efficiency and small-sized double overhung rotor [1]. A typical turbocharger (TC) rotor assembly for the gasoline engine weighs about 0.1 kg, with approximately

L. Wang · A. Wang (✉) · Y. Yin
Light Alloy Research Institute, Central South University,
Changsha 410083, China
e-mail: Longkai.Heat@hotmail.com

L. Wang · A. Wang · X. Heng · M. Jin
State Key Laboratory of High Performance Complex
Manufacturing, Central South University,
Changsha 410083, China

100 mm in length, and has a journal diameter of about 6 mm. For this type of small TC operating at high rotational speed, the floating ring bearing (FRB) is commonly adopted to support the rotor assembly [2]. It can be treated as two plain cylindrical journal bearings in series through a floating ring. Therefore, the inner and outer oil-films have mutual damping effects [3, 4]. Compared with rolling bearings, rolling bearings with SFD, magnetic bearings and tilting-pad bearings, the significant advantage for floating ring bearings (FRBs) is that they are cheaper and easy to produce in large quantities [5]. In comparison with ordinary single film bearings, FRBs have better damping effects and fewer friction losses. However, both inner and outer oil-films can become unstable due to the strong nonlinearity of FRB. Thus, FRBs can induce a variety of self-excited oscillations, which is dependent on the rotor-bearing parameters, especially on the inner and outer bearing clearances. Once the structure design of TC system is unreasonable, sub-synchronous vibrations can exist in a wide speed range [6]. These sub-synchronous vibrations may not influence the safe operation for TC, but they may sometimes be detrimental in terms of generating noise.

The research on TC-FRB system dynamics has been performed so far focusing mainly on the influence of bearing parameters. The nature of the sub-synchronous vibration, bifurcation phenomena and the total instability have been extensively studied in many studies. The classical linear stability analysis can only predict the first bifurcation from the equilibrium position to the limit cycle [7]. It cannot predict the true response of rotor at high speeds, as the static equilibrium position becomes an equilibrium orbit. Due to the complexity of (semi-) analytical bifurcation analyses [8–11], which is not suitable for imperfectly balanced rotors, it is more convenient to use the numerical integration method solving the nonlinear motion equations, to obtain the complete response, and to investigate the stability. Koutsovasilis et al. [12] investigated the effect of FRB on the nonlinear response and the bifurcation during run-up. Using the DYROBES, Bin et al. [13, 14] constructed the FE model of the TC rotor-bearing system and analyzed the influence of the inlet oil temperature and the ring length on the vibration characteristics. Considering the nominal clearance of FRBs in mass production limited to manufacturing capabilities, four different combinations of clearances were also presented to validate

the safe operation of TC [15]. Similarly, the effect of four kinds of limit manufacturing tolerance clearances of FRB on the dynamic characteristics was presented in Ref. [16]. Additionally, variations of bearing clearance induced by temperature have great influence on the amplitude and the sub-synchronous components [17]. Based upon the multi-body dynamics method, the effects of some bearing parameters and operation conditions on the bifurcations have been investigated in Ref. [18, 19]. Tian et al. [20] also investigated the effects of bearing outer clearance on the dynamic characteristics of FRB supported TC rotor. Liu et al. [21] considered the thermal environment on the dynamic behaviors of TC rotor. Due to the strong nonlinearity of FRB, system's motion state may be very complex, the bifurcation analysis from Ref. [22, 23] showed that the TC-journal bearing system response is in a quasi-periodic motion state at high speed. Andres et al. [24] developed computational tools for accelerating product development process of TC. His research focused on the bearing analysis. Due to the high nonlinearity of FRBs, when the rotational speed is large enough, the TC may exhibit total instability, which is the most dangerous unstable state. This phenomenon, reported in Refs. [3, 4, 18–20, 25, 26], can result in the complete destruction to the TC. In a word, the above researches obviously show that the sub-synchronous vibration characteristics, amplitude jump phenomena, system bifurcations, rotor instability characteristics and limit cycle orbits are highly dependent on the TC rotor-FRB structural parameters, lubricating conditions, operation conditions and external loads, etc. For different TC rotor-FRB systems, the results obtained may be diverse. The strong sensitivity indicates that the vibration characteristics of a TC rotor-FRB system can be improved by adjusting the physical parameters. In addition, time transient analysis is a useful tool to be adopted to investigate the rotor dynamic characteristics of TC with FRBs.

Compared with other turbomachines, TCs usually run at very high speeds. Due to the high-speed operation condition and the high nonlinearities introduced by FRBs, even a small difference in unbalance may lead to high vibrations and uncomfortable noises [27]. In order to predict the true response as much as possible, the unbalance force and the bearing nonlinearity must be considered in the modeling process. The goal for engineers is to minimize vibration level

and reduce the dynamics difference over the entire operation speed range, whether it is synchronous or sub-synchronous. The sub-synchronous amplitude of the dominant first mode can be reduced when applying a certain size of unbalance either on the compressor or on the turbine [28]. Bin et al. [29] proposed a suitable level of unbalance to decrease the sub-synchronous vibration of the TC rotor. Wang [30] presented the influence of mass unbalance on the limit cycle orbit. Ma et al. [31] found the unbalance phase can affect the starting speed of instability for a rotor–journal bearing system with two disks. However, these two disks are located within the span of two journal bearings. Namely, the bearing type and the rotor type are completely different from the double overhung rotor. Tian et al. [32] investigated the stability of TC-FRB system with the variations of the unbalance level and unbalance distribution, only involving out-of-phase and in-phase unbalance, and confirmed that they are key parameters for the system response.

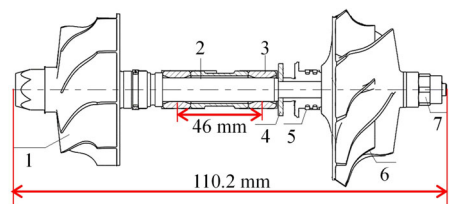
Developing a TC with high efficiency and low vibration demands a thorough understanding of the vibration characteristics under different working conditions. Since the relative phase (orientation) of the unbalance between the turbine and the compressor impeller is random, ranging from 0° to 180° , in practical application, some of the same types of TCs installed on the engines often exhibit a high level of sub-synchronous vibration and uncomfortable noise after they leave the factory with the same balancing process. Due to the compact structure of the TC and the lack of a vibration monitoring system, any form of failure may lead to a catastrophic accident. Existing publications on systematic investigations, discussions and understanding about the influence of the unbalance orientation on the vibration characteristics of the nonlinear TC system have not been found. Furthermore, the dynamics differences of the same type TCs need to be improved. Therefore, it is necessary to perform sufficient studies to reveal the relationship and law between the dynamic characteristics and the unbalance orientation for these TCs, and to suppress the sub-synchronous vibration component in the response as much as possible and maintain the vibration amplitude to an acceptable scope by controlling unbalance orientations. The research can give reasonable understanding on the unbalance orientation effect, and provide some theoretical and technical references for the manufacturing, balancing, fault

diagnosis, and the reduction of vibration and noise for high-speed TCs.

With the design goal of a high-efficient and low-vibration TC, this paper mainly focuses on the effects of the unbalance orientation, which is formed by the two unbalance forces at the nose walls of both impellers, on the suppression of the sub-synchronous vibration components in the response. A realistic TC is taken as the research object, in which the rotor is discretized by using the FE method combined Guyan DOF reduction, and the reaction force of the oil-film is embedded in the TC rotor-ring motion governing equations. Numerical simulations based on the constructed rotor-FRB model and associated experimental comparison were both conducted to verify the reasonability of the model built, and the vibration mechanism with the changing of unbalance orientation is studied.

2 TC rotor-bearing system model

A real TC rotor assembly is shown in Fig. 1. The TC rotor with two identical FRBs under study weighs 104.7 g and has a total length of 110.2 mm. As a double overhung rotor, the turbine and compressor wheels are outboard of two bearings, of which the bearing span is 46 mm. The operating speed can be up to 180,000 r/min. To comprehensively understand the rotor vibration characteristics and the safety under overspeed operation conditions, the maximum speed studied is extended to 230,000 r/min. As a common rule of thumb, the TC exhibits severe vibrations and mechanical failures without a proper rotor dynamics design [33]. In practice, when the rotational speed increases to a certain value, some TCs of the same type installed on car engines may exhibit high levels of sub-synchronous vibration and considerable noise, some TCs, however, never showed up. Aiming at this problem, therefore, it is necessary to perform



1-Turbine 2-Shaft 3-Floating ring 4-Ring 5-Collar 6-Compressor 7-Nut

Fig. 1 Schematic diagram of a TC rotor with FRBs

sufficient studies to reveal the relationship and law between the dynamic characteristics and the unbalance orientation under residual imbalance conditions for these high-speed TCs, which are highly sensitive to the unbalance parameters.

2.1 FRB mathematical model

Both FRBs, as shown in Fig. 2a, are the same in geometric construction and lubricating condition. The FRB has two oil-films [34], i.e., the inner and outer oil-films. The inner oil-film has two rotating surfaces, which correspond to the shaft and floating ring with rotational speeds of Ω_j and Ω_r , while the outer oil-film has only one rotating surface, i.e., the ring with rotational speed of Ω_r . Figure 2b shows the mid-plane cross-sectional view of the FRB. When the rotor is running, the inner oil-film rotating speed is the sum of Ω_j and Ω_r , while the outer oil-film rotates only with Ω_r . The Reynolds equations for both films can be expressed as follows:

$$\frac{1}{R_j^2} \frac{\partial}{\partial \theta_i} \left(\frac{h_i^3}{12\mu_i} \frac{\partial p_i}{\partial \theta_i} \right) + \frac{\partial}{\partial Z_i} \left(\frac{h_i^3}{12\mu_i} \frac{\partial p_i}{\partial Z_i} \right) = \frac{\Omega_j + \Omega_r}{2} \frac{\partial h_i}{\partial \theta_i} + \frac{\partial h_i}{\partial t}, \tag{1}$$

$$\frac{1}{R_o^2} \frac{\partial}{\partial \theta_o} \left(\frac{h_o^3}{12\mu_o} \frac{\partial p_o}{\partial \theta_o} \right) + \frac{\partial}{\partial Z_o} \left(\frac{h_o^3}{12\mu_o} \frac{\partial p_o}{\partial Z_o} \right) = \frac{\Omega_r}{2} \frac{\partial h_o}{\partial \theta_o} + \frac{\partial h_o}{\partial t}, \tag{2}$$

where subscripts i and o are for distinguishing the inner and outer oil-film parameters, respectively.

Subscripts j and r identify the parameters of the journal and floating ring. p denotes the fluid film pressure, μ is the dynamic viscosity, and Ω is the rotationally angular speed in rad/s. R_j and R_{ro} represent the journal radius and the floating ring outer radius, respectively. θ is the angular coordinate in the fixed reference frame. Z denotes the axial coordinate. The oil-film thickness h can be derived as follows:

$$h_i(\theta_i, t) = C_i - x_{jr} \cos \theta_i - y_{jr} \sin \theta_i, \tag{3}$$

$$h_o(\theta_o, t) = C_o - x_r \sin \theta_o - y_r \cos \theta_o. \tag{4}$$

where C is the radius clearance. x and y are the dimensional displacements, and the relative displacements between the journal and floating ring are defined by $x_{jr} = x_j - x_r$ and $y_{jr} = y_j - y_r$.

The oil-film viscosity corresponding to a certain temperature can be obtained by the viscosity–temperature equation. For the lubricant brand SAE 10 W-30, the associated viscosity–temperature curve is depicted in Fig. 3. According to the torque balance equation and the heat balance equation [35, 36], the ring–journal spinning speed ratio and the viscosity of oil-films can be obtained. Once the floating ring speed and the lubricating oil viscosity are known, the two Reynolds equations for the inner and outer oil-films can be solved separately just like the conventional plain journal bearing.

Due to the highly nonlinear nature of FRBs and high-speed operating conditions of journal and floating ring, in order to obtain the true response of the rotor-bearing system, a nonlinear time transient analysis must be performed and the nonlinear oil-film

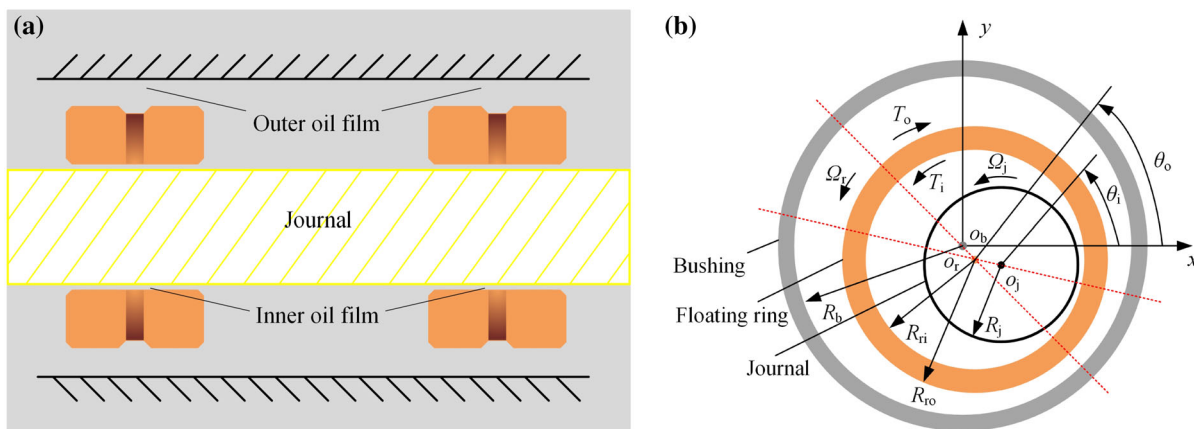


Fig. 2 FRB: **a** schematic diagram, **b** sectional view

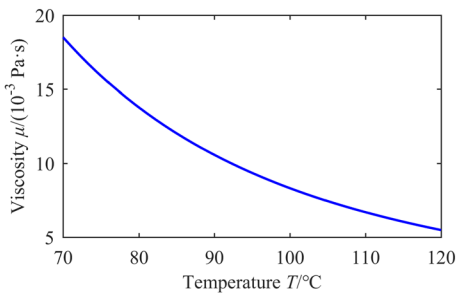


Fig. 3 Viscosity–temperature relationship of SAE 10 W-30

forces should be obtained at every time instant. The nonlinear oil-film forces for the inner and outer fluids can be solved by the FE method or analytic formula [37]. Based on the Capone model [38], nonlinear oil film forces can be expressed as follows:

$$\begin{bmatrix} F_{bxi} \\ F_{byi} \end{bmatrix} = \sigma_i \begin{bmatrix} f_{bxi} \\ f_{byi} \end{bmatrix}, \quad \begin{bmatrix} F_{bxo} \\ F_{byo} \end{bmatrix} = \sigma_o \begin{bmatrix} f_{bxo} \\ f_{byo} \end{bmatrix}, \quad (5)$$

$$\begin{aligned} \sigma_i &= \mu_i (\Omega_j + \Omega_r) \frac{D_j}{2} L_{ri} \left(\frac{D_j}{2C_i} \right)^2 \left(\frac{L_{ri}}{D_j} \right)^2, \quad \sigma_o \\ &= \mu_o \Omega_r \frac{D_{ro}}{2} L_{ro} \left(\frac{D_{ro}}{2C_{ro}} \right)^2 \left(\frac{L_{ro}}{D_{ro}} \right)^2, \end{aligned} \quad (6)$$

where σ is the Sommerfeld coefficient; D_j is the journal diameter, D_{ro} is the outer diameter of floating ring, L_{ri} is the inner length of floating ring, and L_{ro} is the floating ring outer length. The general form of nonlinear oil film force, f_{bx} and f_{by} , can be expressed as follows:

$$\begin{bmatrix} f_{bx} \\ f_{by} \end{bmatrix} = - \frac{\sqrt{(X-2\dot{Y})^2 + (Y+2\dot{X})^2}}{1-X^2-Y^2} \times \begin{pmatrix} 3X \times V(X, Y, \alpha) - \sin \alpha \times G(X, Y, \alpha) - 2 \cos \alpha \times S(X, Y, \alpha) \\ 3Y \times V(X, Y, \alpha) + \cos \alpha \times G(X, Y, \alpha) - 2 \sin \alpha \times S(X, Y, \alpha) \end{pmatrix}, \quad (7)$$

$$V(X, Y, \varphi) = \frac{2 + (Y \cos \varphi - X \sin \varphi) \times G(X, Y, \varphi)}{1 - X^2 - Y^2}, \quad (8)$$

$$S(X, Y, \varphi) = \frac{X \cos \varphi + Y \sin \varphi}{1 - (X \cos \varphi + Y \sin \varphi)^2}, \quad (9)$$

$$G(X, Y, \varphi) = \frac{2}{\sqrt{1 - X^2 - Y^2}} \times \left(\frac{\pi}{2} + \arctan \frac{Y \cos \varphi - X \sin \varphi}{\sqrt{1 - X^2 - Y^2}} \right), \quad (10)$$

$$\varphi = \arctan \frac{Y + 2\dot{X}}{X - 2\dot{Y}} - \frac{\pi}{2} \text{sign} \frac{Y + 2\dot{X}}{X - 2\dot{Y}} - \frac{\pi}{2} \text{sign}(Y + 2\dot{X}). \quad (11)$$

where $X = x/C$ and $Y = y/C$ are the non-dimensional displacements. For the inner and outer oil-films, substituting the corresponding displacement and velocity in Eq. (7), the nonlinear oil-film forces, as described in Eq. (5), can be assembled into the total rotor-bearing system equations for the nonlinear transient response simulation. The details of governing equation of motion for the floating ring were well documented in Ref. [20].

2.2 FE dynamic model of the TC rotor-bearing system

The compressor and turbine impellers (Fig. 4) are regarded as rigid disk models, where the mass and the moment of inertia are listed in Table 1. For research purposes, some reasonable simplifications and assumptions are made on the rotor, such as the non-uniform cross section element is modeled with several cylindrical and conical beam elements [35] and small changes on the chamfering of the rotor-shaft are also ignored. According to the actual structural feature of rotating assembly and assumptions on FRBs, the continuous rotor with two FRBs is discretized by using the FE method and Guyan reduction, as shown in Fig. 5. Each shaft element has four degrees-of-freedom (DOFs) at each node, and the ring is modeled as a pedestal.

The TC rotor is finally modeled with 19 main elements, including 42 sub-elements. Nodes 21 and 22 denote the turbine and compressor end floating rings, respectively. A red five-pointed star between nodes 9 and 10, which is closer to the turbine end bearing, represents the C.G. of rotor. This causes the bearing static load on the turbine end to be ten times that of the compressor end bearing. As a result, the compressor displacement is significantly larger than the turbine end when the rotor is in the second-order mode. Also

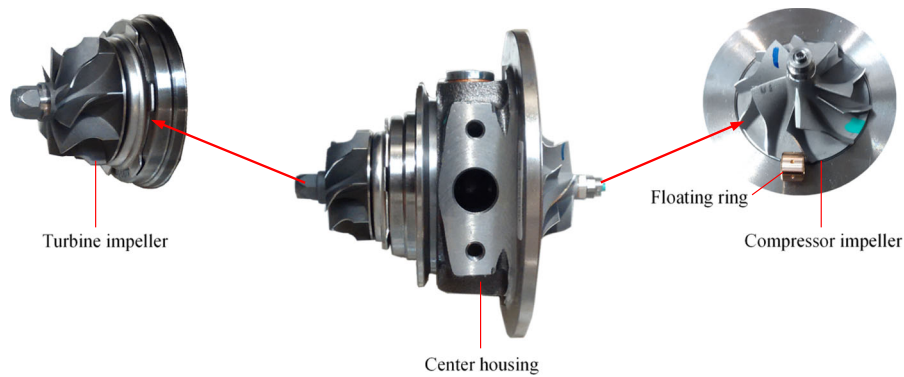


Fig. 4 Automotive turbocharger

Table 1 Parameters for turbine and compressor impeller

No	Component	Mass m (kg)	Polar inertia moment I_p (kg m ²)	Diameter inertia moment I_d (kg m ²)
1	Turbine	0.0607	5.88E-6	8.42E-6
2	Compressor	0.0212	2.76E-6	2.31E-6

shown in Fig. 5, the red arrow indicates the unbalance force applied. For linear analyses, the bearing stiffness and damping coefficients were calculated at the static equilibrium position by selecting the Reynolds boundary condition. However, for the nonlinear time transient simulation, the nonlinear oil-film forces are embedded into the system equations of motion [39]. The governing equations of motion for the TC rotor-FRB system are derived as follows:

$$M\ddot{q} + (C + \Omega G)\dot{q} + Kq = F_i + F_o + F_{ub} + F_s, \tag{12}$$

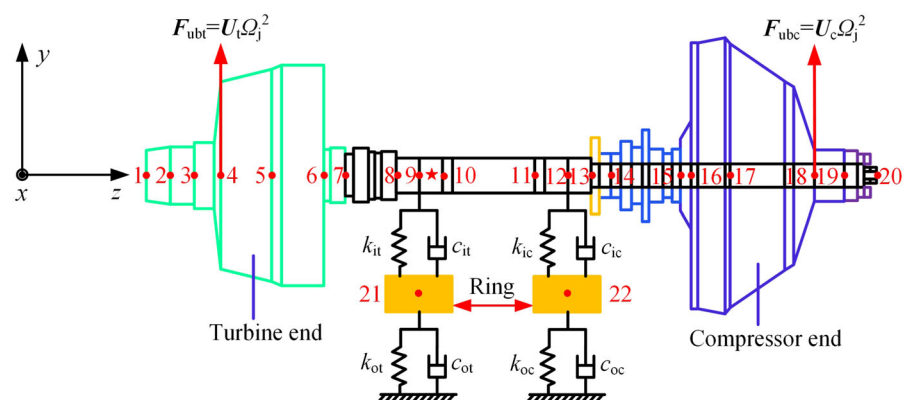
where q is the displacement vector to be solved. M denotes the mass matrix. C represents the damping matrix, and G is the skew-symmetric gyroscopic matrix. K denotes the system stiffness matrix. F_i is the inner oil-film force. F_o represents the outer oil-film force vector. F_s is the gravity vector. F_{ub} is the synchronous excitation due to mass unbalance, which only exists at the nose walls of the compressor (CNW) and turbine (TNW).

$$\begin{bmatrix} F_{ubcx} \\ F_{ubcy} \end{bmatrix} = \begin{bmatrix} U_c \Omega_j^2 \cos(\Omega_j t + \phi_c) \\ U_c \Omega_j^2 \sin(\Omega_j t + \phi_c) \end{bmatrix}, \tag{13}$$

$$\begin{bmatrix} F_{ubtx} \\ F_{ubty} \end{bmatrix} = \begin{bmatrix} U_t \Omega_j^2 \cos(\Omega_j t + \phi_t) \\ U_t \Omega_j^2 \sin(\Omega_j t + \phi_t) \end{bmatrix}, \tag{14}$$

where F_{ubcx} and F_{ubcy} are the unbalance forces exerted on CNW in x and y directions, respectively. F_{ubtx} and

Fig. 5 FE-based discrete model



F_{ubty} are the unbalance forces applied on TNW. U_c and U_t are the residual mass unbalances. ϕ_c and ϕ_t are, respectively, the initial phase angles for the unbalance force applied at nodes 4 and 18. The unbalance orientation between two unbalance forces (see Fig. 6), which exist on the nose wall of two impellers, is defined as follows:

$$\phi = |\phi_c - \phi_t|. \tag{15}$$

3 Model validation

Rotor material properties are shown in Table 2, and the FRB parameters are listed in Table 3. Although the TC rotor system is highly nonlinear, the Campbell diagram and modes based on the linearized model can give valuable information for nonlinear dynamic analysis. Assuming that the bearing was replaced by the linear spring with stiffness of 10^6 N/m, the Campbell diagram and the first three-order mode shapes as well as the corresponding potential energy distribution are shown in Figs. 7 and 8, respectively. The conical mode critical speed, the cylindrical mode critical speed and the shaft bending mode critical speed are, respectively, 13,900 r/min, 35,700 r/min and 159,100 r/min.

It should be mentioned that most of the potential energy for the first mode in which the two impellers are out-of-phase is concentrated on the bearings (see Fig. 8b). For the second mode in which the both impellers are in-phase, there is considerable bending at the middle position of the shaft. This is because the turbine and compressor impeller are located outside bearing span and the rotating shaft is slender.

Figure 8b shows that the energy between the shaft and bearings will be transformed between the first and second order modes. From the first two modes and the energy distribution, it can be seen that the vibration characteristics of the rotor are significantly affected by the loading conditions. In other words, the in-phase unbalance force formed by the turbine and the compressor impeller is difficult to excite the first mode, while the out-of-phase unbalance force is difficult to excite the second mode, and vice versa.

3.1 Case 1: Comparison between the simulation and test data

The synchronous response simulation is performed by applying an unbalance with a magnitude of 0.2 g mm on node 4, and the amplitude–frequency response curve at node 2 is shown in Fig. 9. It can be observed that there is a prominent amplitude peak at around 59,000 r/min and the corresponding amplification factor (AF) is 2.67. According to the API 617 standard, the corresponding peak speed is called the critical speed. Figure 10 represents the vibration shapes at 30,000 r/min and 59,000 r/min. At lower speed, such as 30,000 r/min, the rotor whirls in conical mode shape. At the peak speed (around 59,000 r/min), the cylindrical mode was excited. The reason for this clear peak at the second-order critical point is that the bearing’s control to the second mode is weak, as shown in Fig. 8b, 35% strain energy is concentrated on the rotating shaft. In this case, the bearing damping cannot sufficiently reduce the vibration. Correspondently, the vibration response curve originated from high-speed balancing machine is shown in Fig. 11. There is no doubt that the tested critical speed is about

Fig. 6 Schematic diagram of unbalance orientation

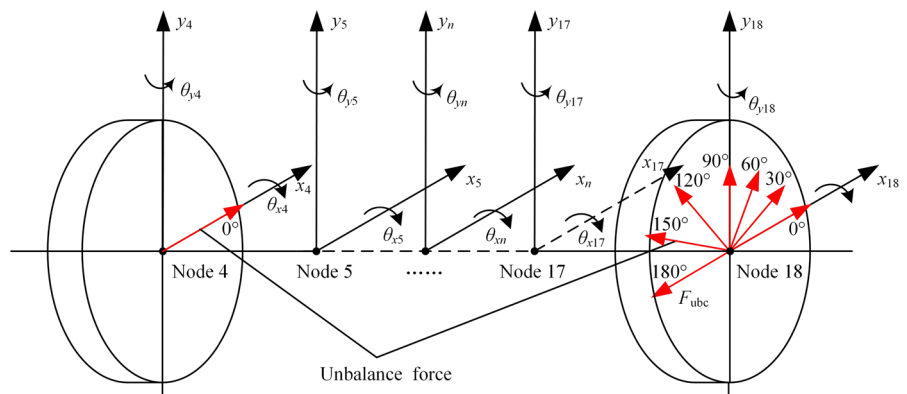


Table 2 Material properties of TC rotor

No	Component	Density ρ /(kg/m ³)	Elastic modulus E /(GPa)	Shear modulus G /(GPa)
1	Shaft	7850	205	80
2	Floating ring	8100	105	40
3	Nut	7800	200	75

Table 3 Physical parameters and lubricating conditions for the FRB

Property	Value	Property	Value
Ring mass/ m_r	2.16 g	Left bearing load/ W_{l0}	0.932 N
Ring inner length/ L_i	3.6 mm	Right bearing load/ W_{r0}	0.095 N
Ring outer length/ L_o	6.15 mm	Oil number	10 W-30
Ring inner diameter/ D_i	6.016 mm	Inner temperature/ T_i	102 °C
Ring outer diameter/ D_o	9.54 mm	Outer temperature/ T_o	95 °C
Journal diameter/ D_s	6 mm	Oil pressure/ p	3.5 Bar
Bearing diameter/ D_b	9.6 mm	Gravity constant g	9.81 m/s ²

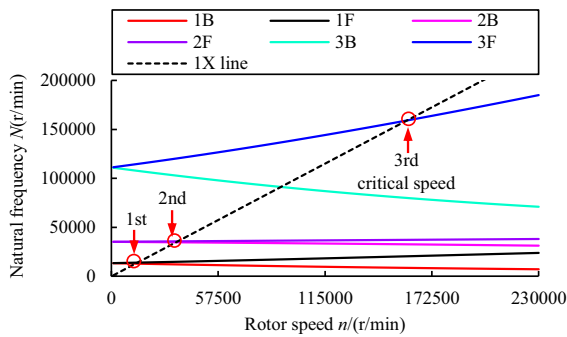


Fig. 7 Campbell diagram

56,000 r/min. Inevitably, there are small differences between the simulation result and the test data. The reason for this is due to the installation error, the machining precision, air flow impact, etc. Overall, the simulation result is in good agreement with the experiment, which verifies the validity of the TC rotor FE model.

3.2 Case 2: Comparison with the existing experimental result

In order to validate the reasonability of the nonlinear response of the dynamic model established by using the proposed modeling method in this paper, the response is solved by using the Newmark-beta algorithm and compared with the published result. As shown in Fig. 12, it can be seen that the spectrum bifurcation sequence between the theoretical simulation and test results [14] has good consistency, which

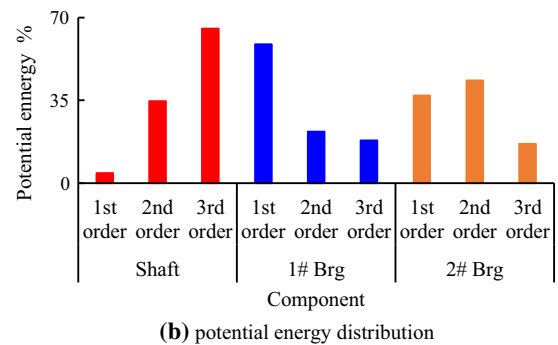
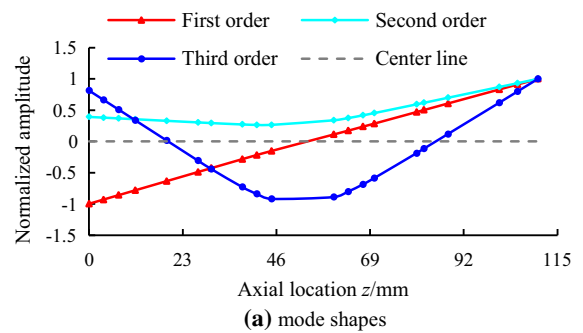


Fig. 8 The first three-order mode shapes and the corresponding potential energy distribution

further shows the effectiveness of modeling method. It should be mentioned that the small difference between Fig. 12b, c are due to the fact that some rotor-bearing parameters are not given in the reference and some thermal bending of the test rotor which causes larger synchronous vibration in experimental results than those predicted by the simulation. However, those

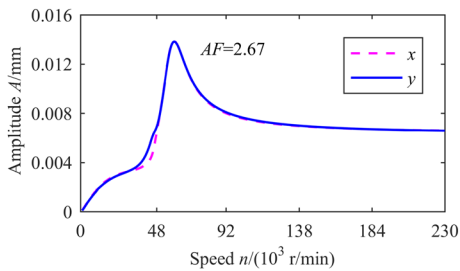


Fig. 9 Amplitude–frequency response curve in both x and y directions based on the FE model

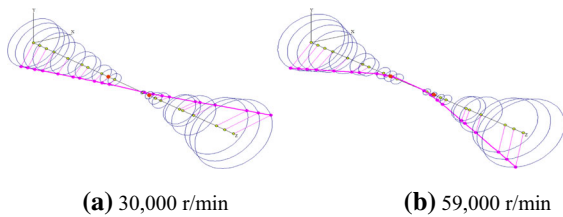


Fig. 10 Vibration shapes at two different rotating speeds

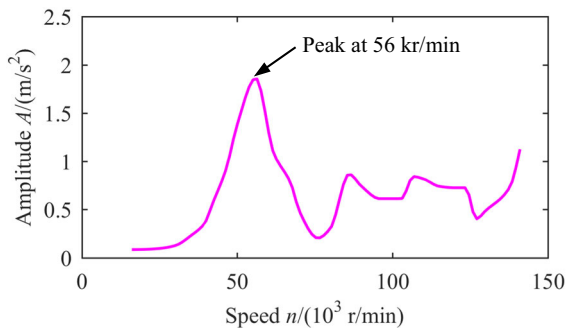


Fig. 11 Vibration response curve from the balancing machine differences do not affect the validity of the model. Therefore, it is reasonable to believe that with the established rotor-bearing model, the theoretical results have good accuracy and meet the research purpose of this paper.

4 Numerical simulations and discussion

In order to predict the complete motion, it is necessary to conduct transient simulation in the time domain [40]. For a high-speed and small-sized TC [41, 42], the rotor dynamic characteristics are closely related to unbalance, which is an unavoidably natural phenomenon. The precession frequency caused by mass unbalance is synchronized with the journal speed. To

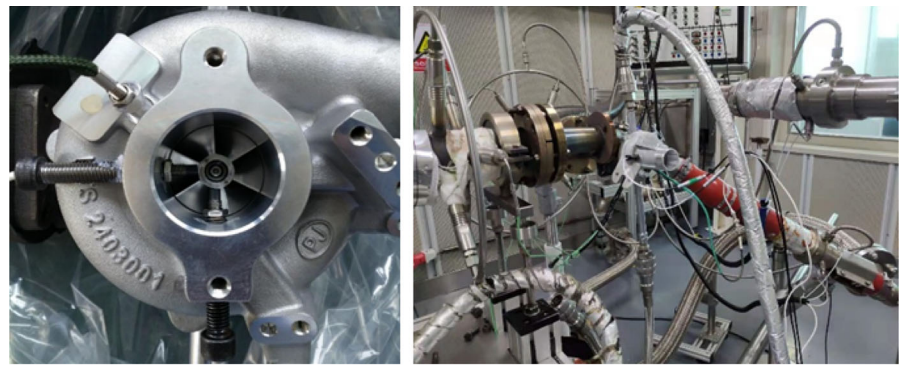
some extent, this fault can be mainly solved by balancing the rotor. However, the self-excited vibration developed during operation is different from synchronous vibration. It does not exist when the rotor is stopping operation. Due to the coupling effect of two oil-films and mass unbalance, the vibration response of TC and its evolution rule become extremely complex.

According to the practical balancing process, the mass unbalances are applied on both nose walls of turbine and the compressor impeller (see Fig. 5 or Fig. 6), respectively. Considering the effects of rotating speed, unbalance orientation and size, the vibration characteristics at node 19 are analyzed and discussed in a rotational speed range from 10,000 r/min to 230,000 r/min. Simulation results with $U_t = U_c = 0.1$ g mm will be presented at first in Sect. 4.1. The results for different magnitudes of unbalance ($U_t = 0.15$ g mm, $U_c = 0.1$ g mm) are shown in Sect. 4.2. Considering the randomness, the orientation between two unbalance forces varies from 0° to 180° . Note that Sub 1 and Sub 2 indicate the sub-synchronous whirling frequencies that are approximately equal to 12% and 57% of the rotor speed, respectively.

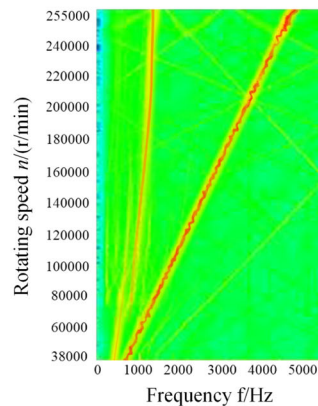
4.1 Effects of the unbalance orientation when $U_t = U_c = 0.1$ g mm

The bifurcation diagram and corresponding three-dimensional (3D) spectrum plot are shown in Fig. 13 for the x displacement under different ϕ at 150,000 r/min. Figure 13a shows that when $\phi < 105^\circ$, the system motion is period-one, and only synchronous (Syn) vibration components can be observed in Fig. 13b. Subsequently, as the unbalance orientation increases, Syn due to unbalance excitation and Sub 1 caused by the outer-film instability coexist in the spectrum, and the amplitude of sub-synchronous vibration component increases rapidly and then exceeds that of Syn. Obviously, the system motion suddenly jumps from period-one into a complex quasi-periodic motion approximately at 106° . The Poincaré maps at $\phi = 0^\circ$ and 180° are illustrated in Fig. 14, and the relationship curves between the amplitude and unbalance orientation are depicted in Fig. 15. These figures confirm the period-one and quasi-periodic motions mentioned above, and indicate the transfer from stability to instability with the change of ϕ . The

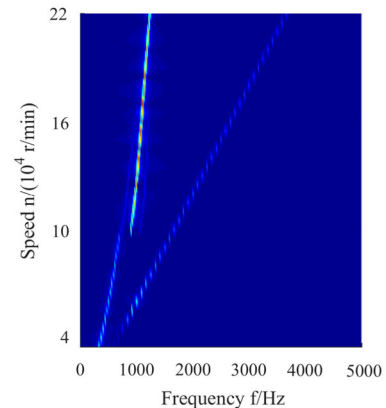
Fig. 12 Comparisons of frequency spectrum: **a** TC rotor system test bench and **b** test result in Ref. [14], **c** simulation result in the present modeling method



(a)



(b)



(c)

above dynamic phenomena imply that some unbalance orientation can induce instability of the outer oil-film and excite the lower system mode.

In order to reveal the vibration mechanism with the changing of unbalance orientation, the 3D motion orbits at 0° , 106° and 180° are depicted in Fig. 16. When the unbalance angle increases, it is of great importance and worth attention that the actual motion shape gradually changes from a simple synchronous mode (combination of the mode shapes of the primary second-order natural frequency and the secondary third-order natural frequency, see Fig. 8a) to a non-synchronous mode (the conical forward mode of Sub 1 due to the instability of outer oil-films). As mentioned in Sect. 3.1, the rigid conical mode (see Fig. 8a), corresponding to the first natural frequency in which the two impellers are moving out-of-phase to each other and the main strain energy (see Fig. 8b) is concentrated on the bearings, is easy to be excited by the 0° unbalance, but difficult to that of 180° . However, the second cylindrical mode, corresponding

to the second natural frequency in which the two impellers are moving in-phase with each other and there is considerable bending on the shaft, is exactly the opposite. It is then clear that the unbalance angle of 0 degree provides very little excitation to the first conical mode, and an angle of 180° provides significant excitation to this mode. As a result, energy between the shaft and bearings is transformed between these modes. This is the main reason why some unbalance orientations can excite the lower system mode and increase the vibration intensity of the rotor system.

From the above analysis, it can be concluded that some unbalance orientations may induce bearing self-excited vibration and excite Sub 1 whirl mode with considerable amplitude. The unbalance orientation is an important parameter that affects the stability, vibration intensity, rotor orbit and motion pattern. Unreasonable unbalance orientation control will make the rotor system change from stable to unstable, and from simple motion to complex motion. At 150,000

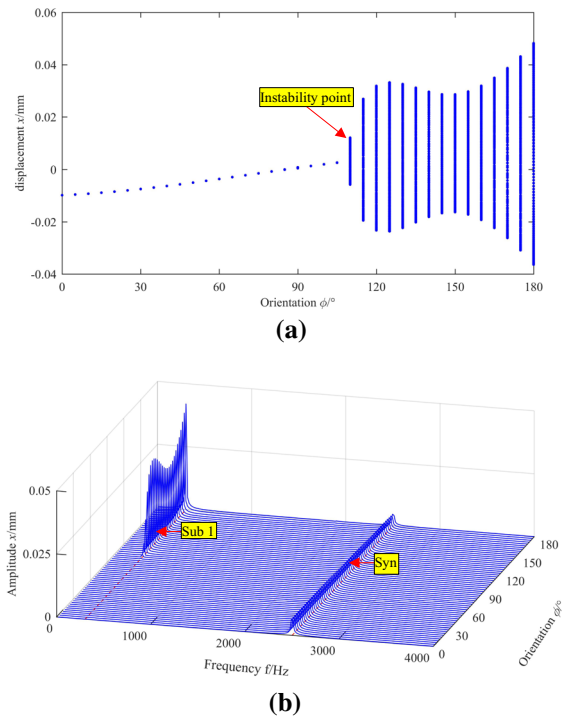


Fig. 13 Vibration response at 150,000 r/min: **a** bifurcation diagram, **b** 3D spectrum diagram

r/min, the ϕ should be within this range from 0° to 105° .

Considering the operating characteristics of the TC rotor with a wide speed range, next, the rotational speed and unbalance orientation are both taken as control parameters to analyze the response. The 3D spectrum plots under different unbalance orientations are presented in Fig. 17, in which Figs. 17a-g are the 3D spectrum plots, and Fig. 17h is the 2D spectrum

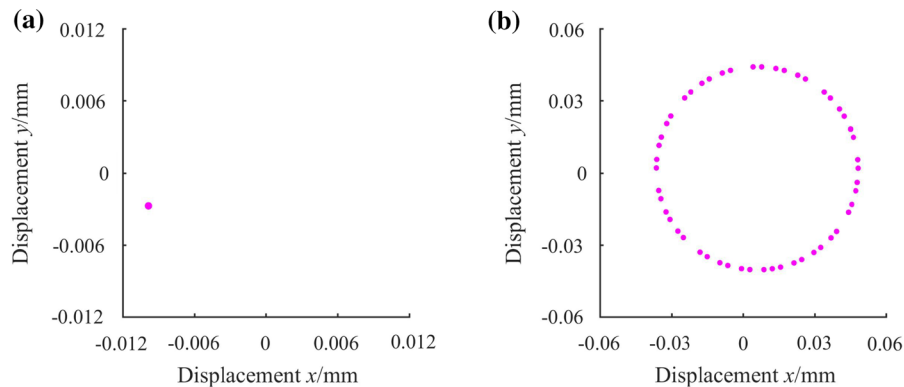


Fig. 14 Poincare maps of the rotor at 150,000 r/min: **a** 0° , **b** 180°

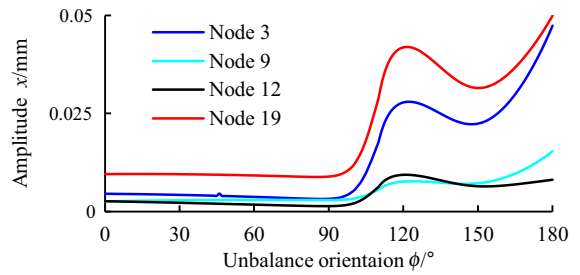


Fig. 15 Relationship curves between amplitude and unbalance orientation at 150,000 r/min

plot at $\phi = 180^\circ$. The total amplitude–speed curves at 0° and 180° are depicted in Fig. 18. The main simulation results are summarized as follows.

- (a) For all of the unbalance orientations, the TC rotor-FRB system is unstable at relatively low speeds. This instability is caused by the whirl of inner oil-films that excite the conical forward mode of Sub 2 component. With the increase in rotational speed, Sub 2 can be safely passed through due to the well damping from the outer oil-film, and the system becomes intermittently stable. The larger the unbalance orientation, the smaller the speed range where intermittent stability exists, or even disappears.
- (b) The changing trend of frequency component under different ϕ is basically consistent except the onset instability speed of Sub 1. This instability is originated from the outer oil-films, and the conical forward mode of Sub 1 is excited. With the increase in unbalance orientation from 0° to 180° , the difference of the onset speed of Sub 1 instability is about 155,000

r/min, which is reduced by 75.61%. As mentioned before, this is because the higher unbalance angles can provide more excitation to the first conical mode. When the first conical mode is excited, the bearings cause the energy transfer between the shaft and the bearings, which leads to an early onset of oil-film instability at higher ϕ .

- (c) With the increase in unbalance orientation, although the synchronous vibration decreases, Sub 1 with higher amplitude increases the total level of the response, as shown in Fig. 18. The reason for this is that the higher unbalance angle provides lower excitation to the second critical cylindrical mode and the third critical bending mode, but provides more excitation to the first critical conical mode. This causes the energy transfer between modes, as shown in Fig. 8b. Although the decrease in the unbalance orientation can improve the instability and vibration level to some extent, at high speeds such as 230,000 r/min, the Sub 1 vibration with considerable amplitude cannot be decreased by simply improving rotor unbalance due to the highly nonlinear dynamic characteristics of FRB, so the rotor vibrates violently.
- (d) When ϕ is larger than 150° , the variation trend of amplitude of Sub 1 with rotational speed is significantly different from that of other ϕ . In the range of 150° to 180° , the larger the unbalance orientation formed, the more obvious the amplitude wave peak appears. The amplitude peak at 180° is nearly three times that of 0° . The reason for the emergency of peak is that the first lateral vibration mode is easily excited at 180° , and coupling effect between the first conical mode and the second critical speed causes the oil-film to be prone to instability.
- (e) Compared with other unbalance orientations, the amplitude of the rotor under the unbalance

Fig. 17. 3D and 2D spectrum plots under different unbalance orientations: **a** 3D spectrum plot at 0° , **b** 30° , **c** 60° , **d** 90° , **e** 120° , **f** 150° , **g** 180° , and **h** 2D spectrum plot at 180°

orientation from 0° to 60° is relatively small, and it does not fluctuate much in the entire design speed range. Therefore, proper control of the unbalance orientation can improve the vibration level and stability of the TC rotor-FRB system to a satisfactory level.

The results show that in the case of residual unbalance, a reasonable range of unbalance orientation will not only improve the stability, but also reduce the amplitude level of the rotor. When the unbalance forces between the turbine and the compressor impellers are controlled within $[0^\circ, 60^\circ]$, the TC can operate relatively well with a smaller amplitude and a higher instability threshold. Controlling the unbalance angle within an appropriate range is an effective method to improve the dynamic characteristics of the TC, and to reduce the vibration difference between the same type of TCs.

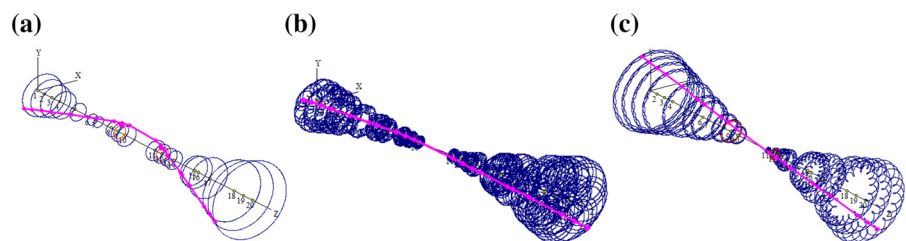
4.2 Effects of the unbalance orientation

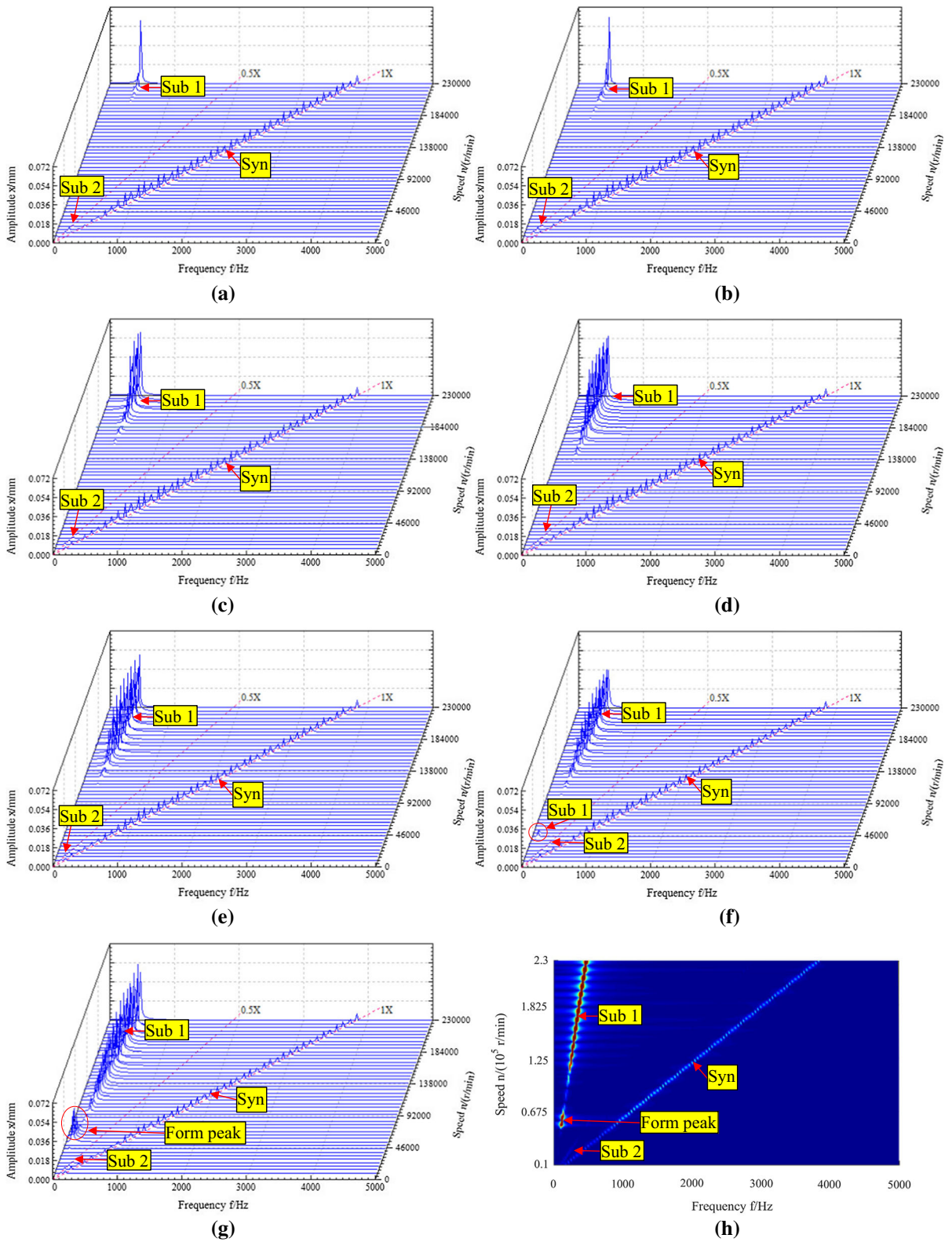
when $U_t = 0.15$ g mm, $U_c = 0.1$ g mm

Aiming at a typical TC design, the turbine wheel is substantially heavier than the compressor. As a result, the magnitude of imbalance on the turbine may be greater than that on the compressor. Different magnitudes of unbalance are imposed on the turbine and compressor wheel ($U_t = 0.15$ g mm, and $U_c = 0.1$ g mm) to obtain the responses (Fig. 19). The conclusions of the obtained results are generally drawn as follows.

- (a) Frequency components of Syn, Sub 1 and Sub 2 can also be observed in spectrums as mentioned before. Besides, the changing tendency of

Fig. 16. 3D motion orbits at 150,000 r/min: **a** 0° , **b** 106° and **c** 180°





frequency components in different unbalance orientations is basically consistent with the results shown in Sect. 4.1.

- (b) The onset speeds of Sub 1 instability at different ϕ have a little difference from those in Sect. 4.1. Obviously, when the unbalance orientation increases, the stability law of the rotor with different magnitudes of unbalance on the two

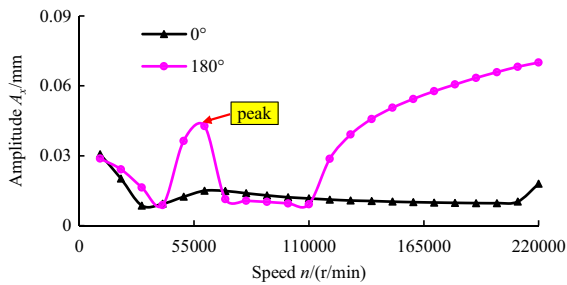


Fig. 18 Total amplitude–speed curves for two extreme unbalance orientations

impellers is also the same as that with the same size unbalance.

- (c) When the unbalance orientation is in the range from 0° to 30° , compared with the previous conditions in Fig. 17a, b, the amplitude of Sub 1 is reduced to a lower level. This is because the increasing synchronous vibration can inhibit the oil-film instability to some extent.
- (d) When the rotor is under the unbalance orientation from 0° to 60° , the amplitude of vibration is relatively desirable and its fluctuation is not large. In this case, the TC operates safely and smoothly in the design speed range (60,000–180,000 r/min). The results are consistent with the previous.

It can be concluded from the above analysis that the influence of the unbalance orientation on the dynamic characteristics of the rotor with different magnitudes of unbalance on both impellers is basically the same as those with the same size unbalance. So, the proposed unbalance orientation control is an effective method to reduce the amplitude and to improve stability.

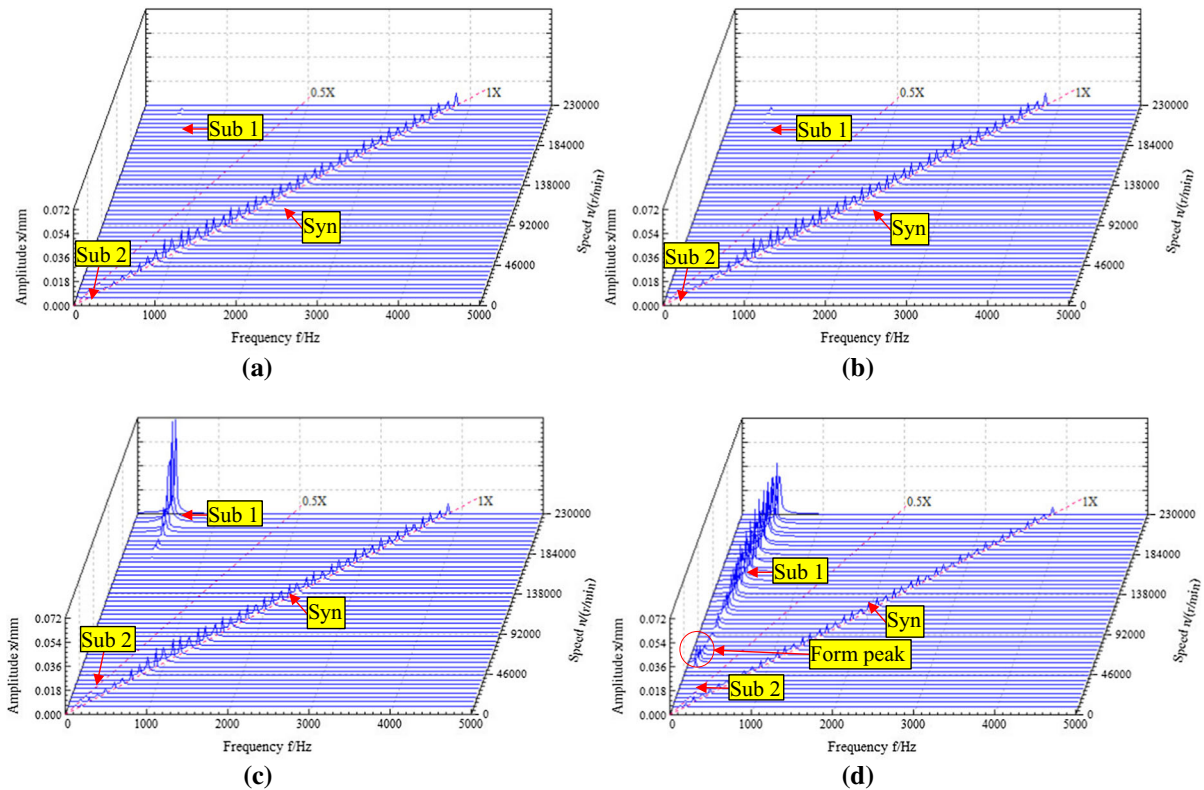


Fig. 19. 3D spectrum plots for $U_t = 0.15$ g mm, $U_c = 0.1$ g mm under different ϕ : **a** 0° , **b** 30° , **c** 60° , **d** 180°

Besides, the research results provide a good explanation for why certain amount TCs of the same type exhibit high levels of sub-synchronous vibration and considerable noise.

5 Conclusions

In order to reveal the reason for the difference in vibration characteristics of the same TC, this paper mainly focuses on the effects of the unbalance orientation on the suppression of sub-synchronous vibration component and the reduction of total vibration intensity. The FE model of a realistic TC rotor-FRB system is built using the discrete element method with Guyan DOF reduction. The nonlinear oil-film forces for the inner and outer fluids are calculated through the formula derived on the basis of the Capone model. On the basis of this, the validity of the modeling method is first verified by the test data. The vibration law changing with the unbalance orientation is revealed for the rotor with the same unbalance magnitude imposed on the nose walls of the turbine and the compressor impeller and then verified by the TC rotor with different magnitudes of unbalance imposed. The main conclusions are shown as follows:

1. The TC rotor-FRB system is unstable at relatively lower speeds due to the Sub 2 instability from inner oil-films. However, with the increase in rotational speed, Sub 2 can be safely passed through due to the damping effect from the outer oil-film. The effect of unbalance orientation on the Sub 2 can be neglected.
2. Sub 1 caused by the outer oil-film instability is the main reason for the severe vibration of the TC during operation. The increase in the unbalance orientation can significantly degenerate the stability of the TC rotor system. With the increase in unbalance orientation from 0° to 180° , the difference of the onset speed of Sub 1 instability is about 155,000 r/min, which reduced by 75.61%.
3. The higher unbalance angle provides lower excitation to the second critical cylindrical mode and the third critical bending mode, but provides more excitation to the first critical conical mode, which causes the energy transfer between the shaft and the bearings, as shown in the mode shapes and corresponding potential energy distribution. This is why a larger unbalance angle can arouse self-excited vibration of the oil-film at a lower running speed.
4. In terms of suppressing rotor instability and reducing amplitude, it is recommended to keep the unbalance orientation at an appropriate range from 0° to 60° . To some extent, the proposed control method about the unbalance orientation can effectively restrain the non-synchronous vibration component, reduce the total vibration level in the speed range designed, and improve the vibration difference for the same type of TCs manufactured in the same factory.
5. The research results provide one explanation for why certain TCs of the same type installed on the same engines exhibit high levels of the sub-synchronous vibration and considerable noise. Accordingly, the unbalance orientation is a critical parameter for the TC, and it needs to be carefully considered during the rotor dynamic analysis, design and the balancing process. Besides, the research can give a further understanding to the nonlinear dynamics of TCs.

Authors' contribution Longkai Wang contributed to writing—original draft, investigation, methodology, validation, funding acquisition. Ailun Wang contributed to editing, funding acquisition. Yijun Yin contributed to writing—review and editing. Xing Heng contributed to data curation, supervision. Miao Jin helped in management and proofreading.

Funding This work was supported by the Major State Basic Research Development Program of China (No. 2013CB035706); the National Natural Science Foundation of China (No. 51175517); the Fundamental Research Funds for the Central Universities of Central South University (No. 2019zzts256); and the Hunan Provincial Innovation Foundation for Postgraduate (CX2015B480).

Data availability All data generated or analyzed during this study are included in this published article.

Declarations

Conflict of interest The authors declare that they have no known competing financial interests or personal relationships that could have appeared to influence the work reported in this paper.

References

- Nguyen-Schäfer, H.: *Rotordynamics of Automotive Turbocharger*. Springer, Berlin (2012)
- Koutsovasilis, P.: Mode shape degeneration in linear rotor dynamics for turbocharger systems. *Arch. Appl. Mech.* **87**, 575–592 (2017)
- Schweizer, B., Sievert, M.: Nonlinear oscillations of automotive turbocharger turbines. *J. Sound Vib.* **321**, 955–975 (2009)
- Schweizer, B.: Oil Whirl, oil whip and whirl/whip synchronization occurring in rotor systems with full-floating ring bearings. *Nonlinear Dyn.* **57**, 509–532 (2009)
- Kirk, R.G., Alsaeed, A.A., Gunter, E.J.: Stability analysis of a high-speed automotive turbocharger. *Tribol. Trans.* **50**(3), 427–434 (2007)
- Tian, L., Wang, W.J., Peng, Z.J.: Dynamic behaviours of a full floating ring bearing supported turbocharger rotor with engine excitation. *J. Sound Vib.* **330**, 4851–4874 (2011)
- Kim, S., Palazzolo, A.B.: Effects of thermo hydrodynamic (THD) floating ring bearing model on rotordynamic bifurcation. *Int. J. Non Linear Mech.* **95**, 30–41 (2017)
- Boyaci, A., Seemann, W., Proppe, C.: Stability analysis of rotors supported by floating ring bearings. In: *The 8th IFToMM International Conference on Rotor Dynamics*, Seoul, Korea, pp. 286–295 (2010)
- Boyaci, A., Seemann, W., Proppe, C.: Bifurcation analysis of a turbocharger rotor supported by floating ring bearings. In: *IUTAM Symposium on Emerging Trends in Rotor Dynamics*, Springer, pp. 335–347 (2011).
- Amamou, A., Chouchane, M.: Non-linear stability analysis of floating ring bearings using Hopf bifurcation theory. *J. Mech. Eng. Sci.* **225**(12), 2804–2818 (2011)
- Tomm, U., Boyaci, A., Proppe, C., Seemann, W., Busch, M., Esmaeil, L., Schweizer, B.: Rotor dynamic analysis of a passenger car turbocharger using run-up simulation and bifurcation theory. In: *Ninth International Conference on Turbochargers and Turbocharging*, London, UK, pp. 335–347 (2010).
- Koutsovasilis, P.: Automotive turbocharger rotordynamics: Interaction of thrust and radial bearings in shaft motion simulation. *J. Sound Vib.* **455**, 413–429 (2019)
- Bin, G.F., Huang, Y., Zhong, X.L., et al.: Effect of inlet oil temperature on vibration characteristics of high-speed light-load turbocharger rotor under long period and variable speed. *J. Mech. Eng.* **56**(11), 131–139 (2020)
- Bin, G.F., Huang, Y., Zhong, X.L., et al.: Study on the influence of floating ring axial length on vibration characteristics of high-speed and light-load turbocharger rotor system. *J. Mech. Eng.* **55**(23), 173–181 (2019)
- Chandrasekaran, P. K., Selvaraj, P. R., Vengala et al.: Investigations on the effect of bearing clearance in turbocharger fully floating hydro-dynamic bearing system. In: *6th ASME Gas Turbine India Conference*, Chennai, India (2019)
- Wang, L.K., Bin, G.F., Li, X.J., et al.: Effects of floating ring bearing manufacturing tolerance clearances on the dynamic characteristics for turbocharger. *Chin. J. Mech. Eng.* **28**(3), 530–540 (2015)
- Smolík, L., Hajžman, M., Byrtus, M.: Investigation of bearing clearance effects in dynamics of turbochargers. *Int. J. Mech. Sci.* **127**, 62–72 (2017)
- Schweizer, B.: Dynamics and stability of turbocharger rotors. *Arch. Appl. Mech.* **80**, 1017–1043 (2010)
- Schweizer, B.: Vibrations and bifurcations of turbocharger rotors. In: *SIRM 2009—8th International Conference on Vibrations in Rotating Machines*, Paper-ID 23, Vienna, Austria, 23–25 February (2009). ISBN 978-3-200-01412-1
- Tian, L., Wang, W.J., Peng, Z.J.: Effects of bearing outer clearance on the dynamic behaviours of the full floating ring bearing supported turbocharger rotor. *Mech. Syst. Signal Process* **31**, 155–175 (2012)
- Liu, Z.H., Wang, R.R., Cao, F., et al.: (2020) Dynamic behaviour analysis of turbocharger rotor-shaft system in thermal environment based on finite element method. *Shock Vib.* **4**, 1–18 (2020)
- Singh, A., Gupta, T.C.: Bifurcation analysis of turbocharger flexible rotor system supported on fluid film bearings. In: *3rd International Conference on Condensed Matter & Applied Physics*, Bikaner, India, (2019)
- Singh, A., Gupta, T.C.: Stability analysis of turbocharger rotor system supported on fluid film bearings. In: *3rd International Conference on Condensed Matter & Applied Physics*, Bikaner, India (2019).
- Andres, L.S., Rivadeneira, J.C., Gjika, K., Groves, C., LaRue, G.: Rotordynamics of small turbochargers supported on floating ring bearings-highlights in bearing analysis and experimental validation. *J. Tribol.* **129**(2), 391–397 (2007)
- Schweizer, B.: Total instability of turbocharger rotors—Physical explanation of the dynamic failure of rotors with full-floating ring bearings. *J. Sound Vib.* **328**(1–2), 156–190 (2009)
- Vistamehr, A.: *Analysis of automotive turbocharger non-linear vibrations including bifurcations*, Master's Thesis, Texas AM University (2009)
- Singh, A., Gupta, T.C.: Effect of rotating unbalance and engine excitations on the nonlinear dynamic response of turbocharger flexible rotor system supported on floating ring bearings. *Arch. Appl. Mech.* **90**, 1117–1134 (2020)
- Kirk, R.G., Alsaeed, A.A.: Induced unbalance as a method for improving the dynamic stability of high-speed turbochargers. *Int. J. Rotating Mach.* Article ID 952869, 1–9 (2011). <https://doi.org/10.1155/2011/952869>.
- Bin, G.F., Huang, Y., Guo, S.P. et al.: Investigation of induced unbalance magnitude on dynamic characteristics of high-speed turbocharger with floating ring bearings. *Chin. J. Mech. Eng.* 31 Article number: 88, 1–11 (2018)
- Wang, L.K., Wang, A.L., Jin, M., et al.: Nonlinear effects of induced unbalance in the rod fastening rotor-bearing system considering nonlinear contact. *Arch. Appl. Mech.* **90**(5), 917–943 (2020)
- Ma, H., Li, H., Zhao, X.Y., et al.: Effects of eccentric phase difference between two discs on oil-film instability in a rotor-bearing system. *Mech. Syst. Signal Process* **41**(1–2), 526–545 (2013)
- Tian, L., Wang, W.J., Peng, Z.J.: Nonlinear effects of unbalance in the rotor-floating ring bearing system of turbochargers. *Mech. Syst. Signal Process.* **34**(1–2), 298–320 (2013)

33. Wang, L.K., Wang, A.L., Jin, M., et al.: Nonlinear dynamic response and stability of a rod fastening rotor with internal damping effect. *Arch. Appl. Mech.* **91**(9), 3851–3867 (2021)
34. Rohde, S.M., Ezzat, H.A.: Analysis of dynamically loaded floating-ring bearings for automotive applications. *J. Lubr. Technol.* **102**, 271–277 (1980)
35. Chen, W.J., Gunter, E.J.: *Introduction to Dynamics of Rotor-Bearing Systems*. Trafford Publishing, Victoria (2010)
36. Chen, W.J.: *Practical Rotordynamics and Fluid Film Bearing Design*. Eigen Technologies, Incorporated (2015)
37. Zhong, Y.E., He, Y.Z., Wang, Z., et al.: *Rotor Dynamics*. Tsinghua University Press, Beijing (1987)
38. Adiletta, G., Guido, A., Rossi, C.: Chaotic motions of a rigid rotor in short journal bearings. *Nonlinear Dyn.* **10**, 251–269 (1996)
39. Friswell, M.: *Dynamics of Rotating Machines*, pp. 102–103. Cambridge University Press, Cambridge (2010)
40. Wang, L.K., Yin, Y.J., Wang, A.L., et al.: Dynamic modeling and vibration characteristics for a high-speed aero-engine rotor with blade off. *Appl. Sci.* **11**(20), 9674 (2021)
41. Tian, L.: Investigation into nonlinear dynamics of rotor-floating ring bearing systems in automotive turbochargers. DPhil thesis, University of Sussex, p 1 (2012)
42. Wang, L.K., Bin, G.F., Li, X.J., et al.: Effects of unbalance location on dynamic characteristics of high-speed gasoline engine turbocharger with floating ring bearings. *Chin. J. Mech. Eng.* **29**, 271–280 (2016)

Publisher's Note Springer Nature remains neutral with regard to jurisdictional claims in published maps and institutional affiliations.